Appl Phys B (2010) 101: 511–521
DOI 10.1007/s00340-010-4281-6

Applied Physics B
Lasers and Optics

Toward single attosecond pulses using harmonic emission from solid-density plasmas

P. Heissler · R. Hörlein · M. Stafe · J.M. Mikhailova · Y. Nomura · D. Herrmann · R. Tautz · S.G. Rykovanov · I.B. Földes · K. Varjú · F. Tavella · A. Marcinkevicius · F. Krausz · L. Veisz · G.D. Tsakiris

Received: 16 July 2010 / Revised version: 20 September 2010 / Published online: 30 October 2010

Abstract We report on investigations of high-order harmonic generation from solid surfaces in the coherent wake emission regime with relativistically intense few-cycle (8 fs) laser pulses. Significant spectral broadening compared to previous experiments with many-cycle pulses and the appearance of substructures on the harmonics are observed that strongly fluctuate from shot-to-shot. Measurements in which the linear polarization was rotated or ellipticity of the laser pulse was varied exhibit a strong dependence of the harmonic emission on the polarization state of the incident pulse. We show that the observed spectral features are ultimately connected to the sub-cycle electron dynamics in the laser-solid interaction and thus proof of the few-cycle nature of the observed harmonic emission. Using a simple model we have investigated the factors that play an important role in the shape of the emitted spectrum.

1 Introduction

It has been recently demonstrated that the harmonic emission emanating from the interaction of intense laser pulses with solid-density plasma possesses a remarkable property, the individual harmonics in the emission spectrum are phase-locked [1, 2]. This conclusion is based on the experimental observation that in the time domain the emitted

P. Heissler (✉) · R. Hörlein · J.M. Mikhailova · Y. Nomura · D. Herrmann · R. Tautz · S.G. Rykovanov · F. Tavella · A. Marcinkevicius · F. Krausz · L. Veisz · G.D. Tsakiris
Max-Planck-Institut für Quantenoptik, 85748 Garching, Germany
e-mail: patrick.heissler@mpq.mpg.de

R. Hörlein · F. Krausz
Fakultät für Physik, Ludwig-Maximilians-Universität München, 85748 Garching, Germany

M. Stafe
Department of Physics, University "Politehnica" of Bucharest, 060042 Bucharest, Romania

J.M. Mikhailova
A.M. Prokhorov General Physics Institute, Russian Academy of Science, 119991 Moscow, Russia

S.G. Rykovanov
Moscow Engineering Physics Institute, 115409 Moscow, Russia

I.B. Földes
KFKI-Research Institute for Particle and Nuclear Physics, 1525 Budapest, Hungary

K. Varjú
Department of Optics and Quantum Electronics, University of Szeged, 6720 Szeged, Hungary

Present address:
Y. Nomura
Institute for Solid State Physics, University of Tokyo, Kashiwa, Chiba 277-8581, Japan

Present address:
D. Herrmann
Lehrstuhl für BioMolekulare Optik, Ludwig-Maximilians-Universität München, 80538 München, Germany

Present address:
R. Tautz
Department of Physics and CeNS, Photonics and Optoelectronics Group, Ludwig-Maximilians-Universität München, 80799 München, Germany

Present address:
F. Tavella
DESY, 22603 Hamburg, Germany

Present address:
A. Marcinkevicius
IMRA America Inc., Ann Arbor, MI 48105, USA

light is bunched in form of a train of sub-laser-cycle duration pulses. Moreover, substantial theoretical [3–8] and experimental [9–15] evidence has been accumulated indicating that the plasma medium additionally exhibits the characteristics required for a source of spatially coherent, extreme ultraviolet (XUV) pulses of attosecond duration and unprecedented brightness. This new source is superior to the one based on the harmonic emission from gaseous media in several aspects. Besides being more efficient, it exhibits no inherent limitation on the laser intensity that can be used. In conjunction with rapid progress in laser technology, the plasma medium holds promise for building a source delivering attosecond pulses [16] with enough intensity to be used in XUV-pump XUV-probe spectroscopy. For most of the envisaged applications, the availability of a single attosecond pulse is desirable [17]. There are two approaches toward this objective. Whereas the first relies on the "intensity gating" technique that requires modern laser systems delivering pulses with some Joules of energy and few-cycle duration [6], the second is based on the "polarization gating" technique [18–20] that can be used with the more readily available conventional laser systems delivering 20–40 fs laser pulses. In both cases, Carrier-Envelope-Phase (CEP) stabilized pulses are necessary [21].

In this work, we report on investigations pertaining to both approaches. Using the high-power Light Wave Synthesizer (LWS) [22, 23] delivering 3-cycle (8 fs), non-phase-stabilized 800 nm, ≈16 TW laser pulses, we were able to observe for the first time high harmonics up to the 20th order (H20) generated by the interaction of few-cycle laser pulses with solid targets. During these investigations, the parameters associated with the laser pulse from the LWS laser system were such that the dominant harmonic emission mechanism appears to be what by now is dubbed as Coherent Wake Emission (CWE) [9, 24]. Generally, CWE prevails for values of the normalized vector potential up to $a_L \approx 1$, which in terms of the focused laser intensity I_L and wavelength λ_L is given by $a_L^2 = I_L \lambda_L^2 / [1.38 \times 10^{18}\ \mathrm{W\,cm^{-2}\,\mu m^2}]$. For values of $a_L \gg 1$ the so called Relativistic Oscillating Mirror (ROM) [3, 4, 15] mechanism is considerably more efficient and the harmonic emission is exclusively due to this process. For intermediate values of $a_L \gtrsim 1$, the two processes can coexist and which one of the two dominates depends sensitively on the shape and gradient of the plasma density profile [12].

The novelty in these investigations is the shortness of the laser pulse in combination with on-target intensities exceeding $10^{18}\ \mathrm{W\,cm^{-2}}$. This constitutes a step toward realization of "intensity gating" for the harmonic emission from solid targets. As in the case of gaseous media, the reduction of the number of cycles under the laser pulse envelope would inevitably lead to fewer attosecond pulses in the generated train [17]. Furthermore, only those cycles within the pulse with enough instantaneous intensity would produce harmonic emission in the necessary spectral range for attosecond time scale emission. In this context, harmonic generation using the plasma medium is more favorable because only one attosecond pulse per laser cycle is produced instead of two as in the case of a gaseous medium. Under these circumstances however, some new effects appear that have not been observed before. For example, it is found that the laser pulses are short enough for effects like random Carrier-Envelope-Phase (CEP) fluctuations to manifest themselves in the observed harmonic spectra. The experimental results are analyzed in terms of a simple model supported by 1D PIC (Particle-In-Cell) simulations. The performed analysis not only explains the main features of the experimental results, but more importantly sheds light on the microscopic electron dynamics responsible for the harmonic emission. The "polarization gating" technique has been also proposed as a method to generate single attosecond pulses [19, 20]. To ascertain the appropriateness of the polarization manipulation to achieve a temporal "gate", a detailed study of the harmonic emission in the CWE regime is undertaken in which (a) the polarization between *s*- and *p*-polarized light and (b) the ellipticity of the incident laser pulse was varied. The results are in agreement with PIC simulations and indicate that the first method appears to be quite promising.

2 Experimental investigation of the harmonic emission

The experiments were carried out using the unique few-cycle Light Wave Synthesizer (LWS) [22, 23], which is a Noncolinear Optical Parametric Chirped Pulse Amplification (NOPCPA) system. During these investigations the light source was upgraded from 8 TW (LWS-10) to 16 TW (LWS-20) peak power output. A schematic of the layout of the LWS system is shown in Fig. 1. The Nd:YAG pump laser after frequency doubling delivers 78 ps pulses of 0.5 J in case of LWS-10 and 1 J in case of LWS-20 energy at 532 nm and is optically synchronized to the titanium:sapphire front end (Femtopower, Femtolasers GmbH). The 1 kHz front end produces 25 fs, 800 µJ pulses that are broadened in a hollow-core fiber filled with 2 bar neon to seed the NOPCPA. A grism based stretcher introduces negative group delay dispersion and elongates the pulses to 45 ps that are partially compressed to about 25 ps in an acousto-optical programmable dispersive filter (DAZZLER). The non-collinear optical parametric amplification from 700 nm to 980 nm takes place in two consecutive single-pass Type I BBO stages. In case of the LWS-20 laser system, the pulses are amplified from a few µJ after the DAZZLER up to 1 mJ in the first stage and up to 170 mJ in the second stage. After a bulk compressor including 160 mm SF57 and 100 mm Quartz, an adaptive mirror and a wavefront sensor in a closed loop

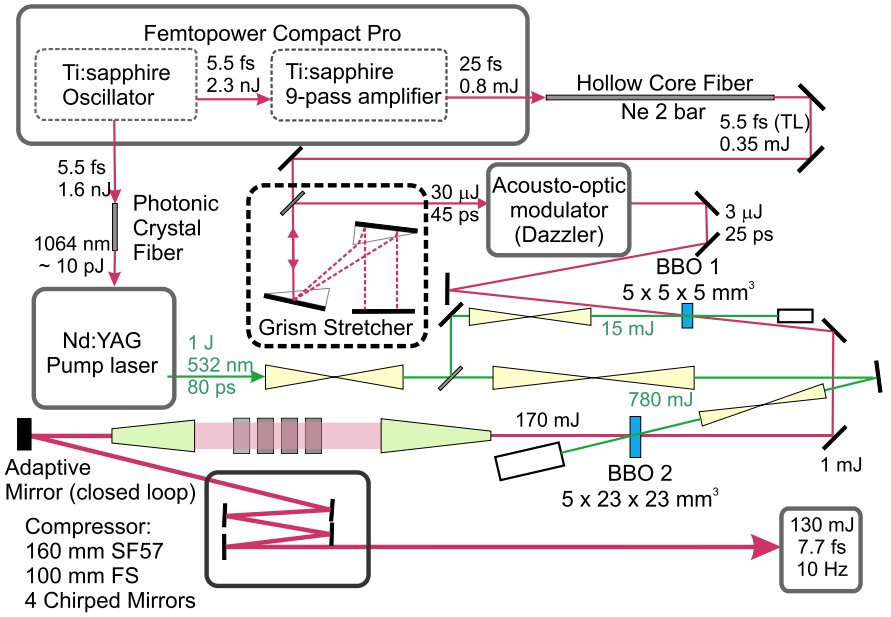

Fig. 1 Layout of the Light Wave Synthesizer 20 (LWS-20) laser system [23]

configuration optimize the focusability. The pulses are sent to a vacuum chamber, where four positively chirped mirrors compress them to a typical intensity Full-Width-Half-Maximum (FWHM) duration of 8 fs, which for the 800 nm center wavelength results in sub-3 optical cycles. Accordingly, the E-field of the pulse has a FWHM duration of $\tau_L = 4.2$ laser cycles. The compressed energy is up to 130 mJ (65 mJ in the case of LWS-10) corresponding to 16 TW (8 TW) power.

Figure 2(a) shows schematically the experimental setup. The laser was focused onto the target at 45° angle of incidence using an F/3, 30° off-axis parabola (effective focal length $f_{\text{eff}} = 168$ mm). In case of LWS-20, the average focused intensity inside a focal spot radius containing 86% of the total energy, was $a_L \approx 1.5$. The corresponding peak intensity is estimated to be $a_L^{\text{peak}} \approx 3$. The measured laser pulse contrast was 10^{-4} at 3.3 ps and 10^{-8} at 5 ps before the peak [23]. The 120 mm diameter fused silica disc targets were mounted on a rotating mechanism allowing the acquisition of approximately 3500 shots at a repetition rate of up to 10 Hz. The generated harmonic radiation in the specular direction was recorded using a grazing-incidence imaging XUV spectrometer equipped with a CsI coated MCP detector. Except for the measurements where the laser polarization was varied (see Sect. 3), the rest of the data were obtained with p-polarized laser beam. An example of a raw data record is shown in Fig. 2(b). The investigated spectral range was 40–100 nm, which for a laser wavelength of 800 nm corresponds to 8th–20th harmonic orders (H8–H20).

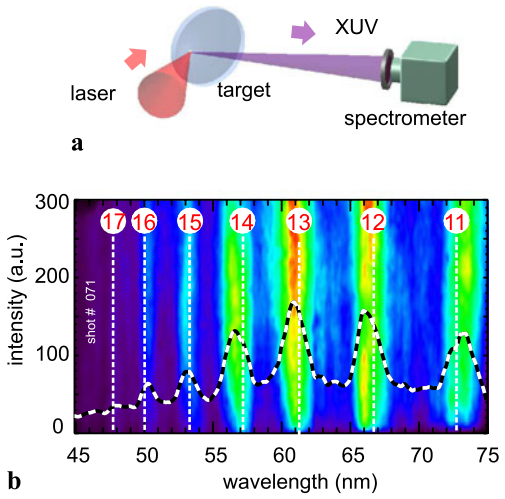

Fig. 2 (**a**) Schematic of the experimental setup, (**b**) raw data record obtained with the grazing-incidence imaging XUV spectrometer

2.1 Harmonic spectrum with 3-cycle laser pulses

Figure 3 shows a set of six single-shot harmonic spectra obtained with our 3-cycle laser pulses in the H11–H16 spectral range. In a more detailed spectral scan a distinct cutoff in the harmonic spectra at H20 was observed. This corresponds to the highest harmonic that the plasma density can sustain confirming that indeed CWE is the dominant harmonic generation process [9]. This is further supported by PIC simulations conducted with parameters close to the ones in the experiment. The measured spectra in Fig. 3 correspond to single laser shots recorded under nominally the same laser conditions. Two distinct characteristics in the spectra are noticeable. The individual harmonics are broadened compared to those from a longer pulse [1, 2, 9, 13] and exhibit from

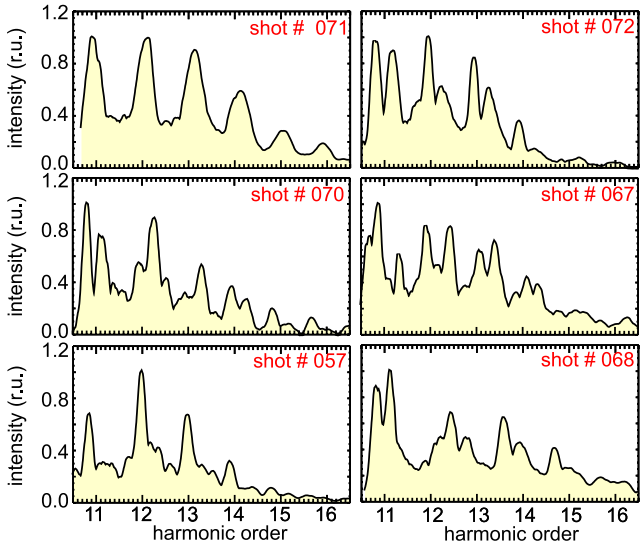

Fig. 3 Single-shot harmonic spectra from fused silica targets. These six records were selected form a set of consecutive shots obtained under nominally same conditions where all the controllable laser parameters were kept fixed. The irreproducible substructure due to CEP variation is clearly visible

shot to shot a strongly irreproducible substructure and a significant spectral shift. Although broader harmonics are expected due to the shortness of the laser pulse, the complex and from shot-to-shot strongly varying spectral structure is a new feature not observed in measurements with longer laser pulses [1, 2]. As discussed in the next Sect. 2.2, the same well behaved spectra exhibiting single harmonic peaks were also observed with the present laser system using positively chirped pulses. This is unequivocal proof that the structure observed with 3-cycle pulses is due to the shortness of the laser pulse.

2.2 Pulse duration variation

The variation of laser pulse duration was accomplished by manipulation of the Group-Delay-Dispersion (GDD) using the DAZZLER incorporated into our laser system (see Fig. 1), i.e., by introducing a chirp in the frequency spectrum of the pulse. This way pulse durations from the nearly Fourier-Transform-Limited (FTL) value of 8 fs to (chirped) pulses of several tens of fs were readily generated.

Figures 4 and 5 depict the main characteristics of the harmonic emission for different pulse durations. They also provide another proof of the fact that the complex structure of the harmonics is due to the shortness of the driving laser pulses. The results indicate that, in contrast to the shortest driving pulse of 8 fs which leads to a complex structure of the harmonics that varies from shot-to-shot (see Fig. 3), the longer pulses obtained by introducing positive chirp values lead to reproducible single peaked harmonics. This is clearly seen in Fig. 4 where a direct comparison of the harmonic spectra for four values of GDD is shown. For nominally FTL pulses (shot # 611), as already discussed, the harmonic spectra appear to be very sensitive to the random variations of CEP when using non-phase-stabilized pulses of only three optical cycles under the envelope (8 fs). For positive values of GDD (shot # 617 and 622) the spectra become progressively narrower and more reproducible. The insusceptibility of the spectrum on the CEP for long, chirped pulses manifest itself in the same way as in the case of experiments on high-harmonic generation on solids and gases with long, FTL pulses. For negative values of GDD (shot # 628) the individual harmonics become even broader and fluctuate even stronger than with FTL pulses. This behavior for different GDD values has been observed before with longer laser pulses [13] and it is attributed to the compensation of the intrinsic harmonic chirp for positive values of GDD. The origin of the intrinsic harmonic chirp is the unequal spacing of the individual pulses in the attosecond pulse train and it is discussed in detail in Sect. 4. In case of uncompensated negative GDD the intrinsic chirp is further increased and the shape of the individual harmonics depends even more sensitively on the CEP variation.

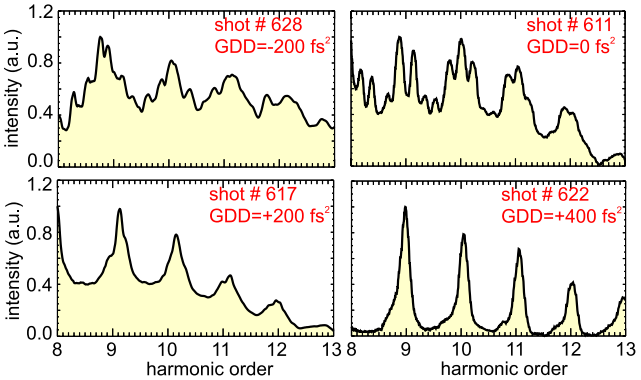

Fig. 4 Harmonic spectra obtained for different values of GDD corresponding to negative chirp (shot 628), no chirp (shot 611) and positive chirp (shots 617 and 622)

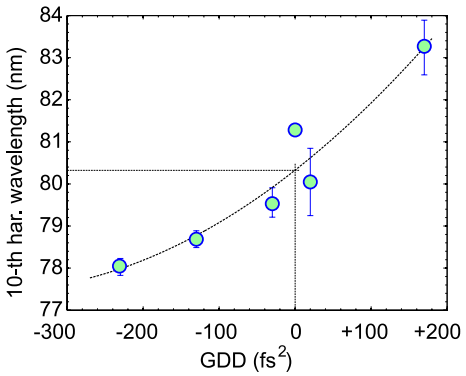

Fig. 5 Dependence of the H10 wavelength on GDD. *The line* is a fit through the experimental points (*circles*)

Another interesting effect observed under variation of the chirp of the laser pulse is the shift of the central wavelength of the individual harmonics. Namely as the GDD value increases the central wavelength also increases. This is depicted in Fig. 5 for the H10. This is attributed to the fact that harmonics are produced predominantly during a particular part of the laser pulse where the intensity is high. As a consequence for a particular value of GDD different parts of the spectrum are responsible for the harmonic generation.

3 Spectral measurements with polarization variation

The dependence of the harmonic emission on the polarization of the incident driving laser pulse is not only interesting from a fundamental point of view but also in connection with the polarization gating technique as a means of generating single attosecond pulses. A number of reports have investigated this subject already theoretically [3, 20, 25, 26] and experimentally [27–31], but no clear picture for the CWE regime has been established so far. In previous reports with long laser pulses or existent prepulses, Rayleigh–Taylor instabilities of the preplasma caused strong surface rippling and therefore polarization scrabbling thus diminishing the effect of changing polarization of the incident laser. However, in our case the shortness and the good contrast of the used laser pulse preserves a clean interaction surface. Since the early theoretical works of Lichters et al. [3] it is well-known that for the polarization dependence of high-harmonics generation certain selection rules apply. In general it was found that the polarization of the generating laser pulse might influence both the intensity and the polarization state of the generated harmonics. In the case of investigations with short-pulse lasers (i.e. shorter than 100 fs) harmonics have only been observed for p-polarized incoming beam. This is expected for the CWE mechanism in which case the existence of an E-field component in the plane of incidence is essential to drag electrons out of the solids (see discussion in Sect. 4). The experiments cited previously aimed primarily at determining the harmonic intensity dependence on the two major polarization directions (s and p) of linearly polarized laser pulses. On the other hand, it is also of interest to investigate experimentally the dependence of the harmonic emission for arbitrarily directed linearly polarized laser light and as a function of the degree of ellipticity. The aim of the present experiment is to obtain a detailed picture of polarization dependence of harmonic generation in the CWE regime. This will provide valuable information regarding the applicability of the polarization gating to generate single attosecond pulses.

The use of the LWS 20 laser system with its polarization insensitive bulk glass and chirped mirror compressor enabled us to change the polarization by inserting small aperture waveplates directly into the unexpanded beam of the laser system where the pulses are still stretched. The polarization state of the laser radiation has been measured at target position, to exclude any influence of the transmission through the compressor and the beamline.

3.1 S–P variation

For measuring the effect of the polarization of the incident laser radiation on the harmonic generation process a commercial broadband, achromatic, zeroth order half-wave plate has been introduced into the laser beam. The plate was rotated in steps of 4 degrees and for every step around 30 spectra in the range of H8 to H13 were recorded with the grazing-incidence spectrometer (see Fig. 2). These spectra have subsequently been integrated over the given harmonic range and averaged. In Fig. 6 the resulting values are shown.

A maximum is observed around fully p-polarized incident laser light. But by rotating the polarization plane to increase the E_s/E_p ratio, the efficiency of the harmonic generation is dropping rapidly to less than 1%, which is around the detection limit of our spectrometer. This behavior is expected, since we are looking at harmonics produced by the CWE mechanism, whereby electrons are accelerated out of the plasma by the component of the incident electric field perpendicular to the target surface. By rotating the half-wave plate in the laser beam, this p-component is decreasing in favor of an increasing s-component while leaving the overall intensity on target constant. This behavior is reproduced by the PIC simulations discussed in detail in Sect. 4.3.

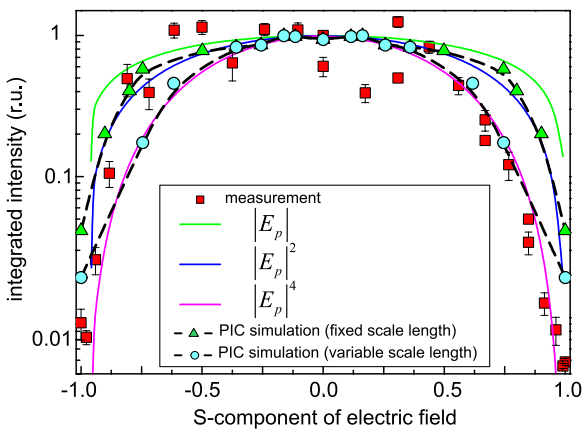

Fig. 6 The effect of the polarization variation from S to P and back to S on the harmonic emission. *The squares* represent the measured values with the error bars being 1 SD over 30 spectra. *The triangles* and *the circles* are the results of PIC simulations with fixed and variable scale length for the preplasma (see discussion in Sect. 4.3). *The curves* indicate the expected dependence $\propto |E_p|^n$ for $n = 1, 2, 4$

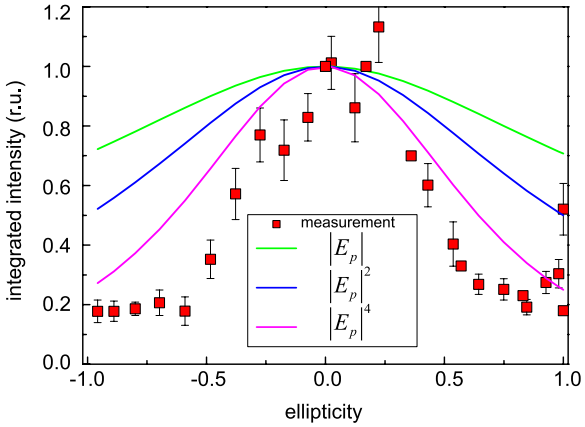

Fig. 7 The effect of the ellipticity variation on the harmonic emission. Points represent the measured values with the error bars being 1 SD over 30 spectra. *The curves* indicate the dependence $\propto |E_p|^n$ for $n = 1, 2, 4$

3.2 Ellipticity variation

Similar to the linear polarization measurement the dependency of the harmonic emission on the incident laser pulse ellipticity has been measured. This measurement was accomplished by replacing the half-wave plate with a zero order quarter wave plate, which also has been rotated in steps of 4 degrees to change the polarization of the transmitted laser beam from circularly polarized on target to linearly p-polarized and back to circular by a rotation of the plate by 90°. Again around 30 spectra of the emitted harmonics in the H8–H13 range have been recorded at each position.

In Fig. 7 the integrated and subsequently averaged values of the spectral intensity are shown. As expected, a clear maximum of the harmonic emission is observed for linearly p-polarized light on target. The intensity of the emitted harmonics is dropping rapidly to around 20% of the peak value with increasing ellipticity. Similar to the case of changing from s- to p-polarization, the reduction in efficiency is much faster than expected when considering just the reduction of the component of the driving electric field perpendicular to the target surface (see discussion in Sect. 4.3).

4 Theoretical analysis and discussion

We first investigate some aspects of the Coherent Wake Emission (CWE) mechanism [1, 2, 9, 12–14], which as already discussed, appears to be the dominant harmonic generation process in our experimental studies. In this regime, several features in the emission spectrum can be understood in terms of a *3-step model* that describes the coherent subcycle dynamics of the plasma electrons.

4.1 The 3-step model

According to this model, which is reminiscent of the 3-step model for the harmonic generation in atoms [32], the interaction unfolds as follows: (i) first, the E-field component perpendicular to the target of the obliquely incident, p-polarized laser pulse launches electrons into the vacuum (Brunel electrons [33]), (ii) depending on the E-field phase during the ejection some of these energetic electrons are then hurled back into the plasma during the second half-cycle of the laser period and form bunches that pass through a density ramp, (iii) this gives rise to resonantly driven plasma oscillations at positions x_q within the density gradient where an integer multiple of the driving frequency ω_L coincides with the local plasma frequency ω_p, i.e., where $q\omega_\mathrm{L} = \omega_\mathrm{p}(x_q)$. At these resonance positions, the excited plasma waves undergo linear mode conversion into EM-waves via inverse resonance absorption [34].

Following the formulation of [33], the electron dynamics can be described in a simplified fashion by the one-dimensional equation of motion along the x-axis (with $x = 0$ on the plasma–vacuum interface). Since we deal with mildly relativistic intensities, i.e., $I_\mathrm{L} \simeq 10^{18}$ W/cm^2, we write the equation of motion in its relativistically correct form. Each single electron moves in the combined E-field of the laser and electrostatic field due to space charge accumulation:

$$\frac{d\beta}{dt} = 4\pi \sin(\Theta) a_\mathrm{L} \left(1-\beta^2\right)^{3/2} \times \left[E_\mathrm{L}(t+t_0)\cos\left(\omega_\mathrm{L}(t+t_0+\varphi)\right) - E_\mathrm{L}(t_0)\cos\left(\omega_\mathrm{L}(t_0+\varphi)\right)\right], \quad (1)$$

with x the distance from the interface in wavelengths λ_L, $\beta = dx/dt$. Here $E_\mathrm{L}(t) = \exp(-t^2/0.72\tau_\mathrm{L}^2)$ is the temporal envelope of the laser E-field, Θ the angle of incidence, and $\omega_\mathrm{L} = 2\pi$ the laser frequency. The time t, t_0 and the FWHM intensity pulse duration τ_L are in laser periods T_L and the CE-phase φ is normalized to 2π. The last term in (1) represents the effect of the space charge to the electron motion as formulated in [33]. The instant of release of the electron from the plasma–vacuum interface is denoted as t_0. In the relativistically correct equation of motion we have neglected the magnetic field term to keep the model simple and one-dimensional. As PIC simulation confirm, for mildly relativistic intensities this is justified. A similar analysis but with emphasis on the escaping electrons has been reported in [35]. The numerical solution of (1) for $a_\mathrm{L} = 1.5$, $\tau_\mathrm{L} = 3$ and $\Theta = 45°$ is depicted in Fig. 8(a). The electrons at the vacuum–plasma interface are initially at rest and uniformly distributed, i.e. t_0 is varied in equidistant intervals. After reentry into the plasma region they are assumed to travel at the constant velocity acquired during the excursion

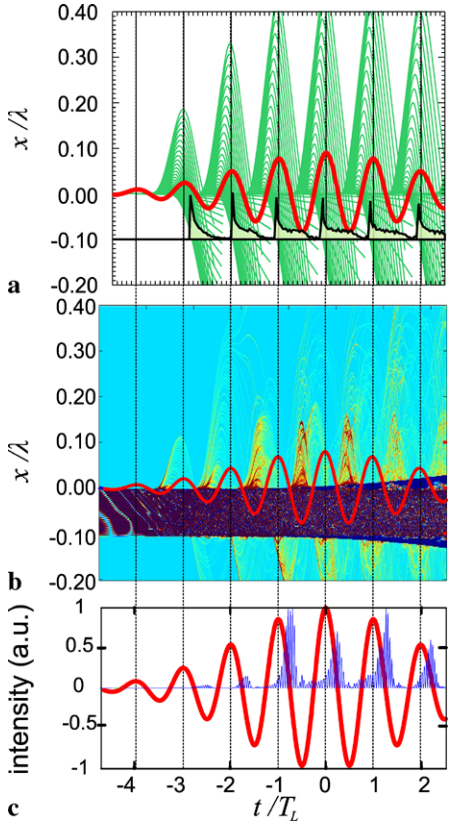

Fig. 8 (**a**) Numerical solution of (1). The trajectories of the electrons released into the vacuum at uniformly varying values of t_0 and returning to the plasma surface are shown *in green* and the histogram (number of electrons per unit time) at a depth of $x = -0.1$ is plotted *in black line* (*yellow filled*). For reference the driving electric field is also plotted (*red line*). (**b**) The electron density evolution for few cycles at the beginning of the pulse obtained from the 1D-PIC simulation and the E-field of the driving pulse (*red*). The density is color coded with the solid-density target slab appearing as a *dark bar*. (**c**) The generated as-pulses (*blue*) are positioned at the point in time coinciding with the return of the expelled electrons

in the vacuum. In Fig. 8(a) only those orbits of the electrons returning to the plasma region are plotted. The histogram of the electrons per unit time crossing a line located at $x = -0.1$ behind the interface clearly shows a temporal bunching of the returning electrons within a time window amounting to a fraction of a cycle. The reason for this bunching is merely the electron dynamics for different phases of the sinusoidal E-field of the laser. A careful examination of the orbits in Fig. 8(a) indicates that at the beginning of each cycle (positive-to-negative field crossing) some electrons are pulled out but due to the weak field their excursion is short. As the field continues to grow, the subsequent electrons move further from the surface but due to their higher velocity they return approximately at the same time with the previous ones. This results in a crossover of the orbits inside the plasma and the formation of electron bunches. Since the harmonics are generated via these bunches of energetic electrons (e-bunches), the emission time of the individual attosecond bursts will follow the occurrence of the electron temporal localization.

We have further substantiated the validity of our simple *CWE 3-step model* by performing simulations using the 1D PIC code PICWIG [20]. The input parameters used were close to those in the experiment, namely $a_L = 1.5$, $\Theta = 45°$ and $n_e/n_c = 400$ where n_e is the maximum electron density and n_c is the critical electron density corresponding to the frequency ω_L of the driving laser pulse. The laser spot size is estimated to be $\backsimeq 7$ μm, which is larger than the length of the 3-cycle laser pulse of $\backsimeq 2.4$ μm. This indicates that the interaction is nearly one-dimensional and thus the use of 1D PIC code is justified. We chose to conduct the simulations at the average intensity in the interaction area to approximate the behavior of the whole focal region. Furthermore, for the calculation of the harmonic emission a linear density ramp with a scale length of $L = 0.2\lambda_L$ was assumed in front of the plasma slab. This value is based on a simple estimation in which an expansion velocity of 5×10^7 cm/s is assumed and as expansion interval the point of 10^{-4} contrast at 3.3 ps before the peak of the laser pulse, i.e. the point where plasma is generated. The electron density evolution due to a $\tau_L = 3$ (FWHM in intensity) laser pulse of those electrons returning to the plasma for few cycles at the beginning of the pulse is depicted in Fig. 8(b). It exhibits an almost quantitatively similar behavior as the one deduced using the CWE 3-step model (compare Fig. 8(a)). In particular, the time interval during which most of the electrons are pulled into vacuum is preferentially near the first quarter cycle after each positive-to-negative zero crossing of the electric field and their return half a cycle later as predicted by the model also. The attosecond pulse train generated by the coherent superposition of the H10 to H20 harmonics is shown in Fig. 8(c). This confirms the postulation that the harmonic emission contributing to the formation of attosecond pulses occurs at the points in time that coincide with the return of the expelled electrons. From this comparison it becomes apparent that the CWE 3-step model despite its simplicity contains most of the relevant physics.

The change in the oscillation amplitude due to the envelope of the driving pulse gives rise to another effect, which for moderate laser intensities $a_L = 0.2$ and longer pulses has been investigated before using PIC simulations [13]. As is clearly seen in Fig. 8(a), the e-bunches are not equidistant. The distance between them monotonically increases with time while the time interval Δt_n between the nth positive-to-negative zero crossing of the E-field and the resulting e-bunch decreases on the rising edge of the pulse but then increases again. Figures 9(a) and 9(c) show the data points extracted from the corresponding histograms for the unequally spaced e-bunches generated by a 15-cycle and 3-cycle laser pulse. For a Gaussian pulse envelope the data points follow

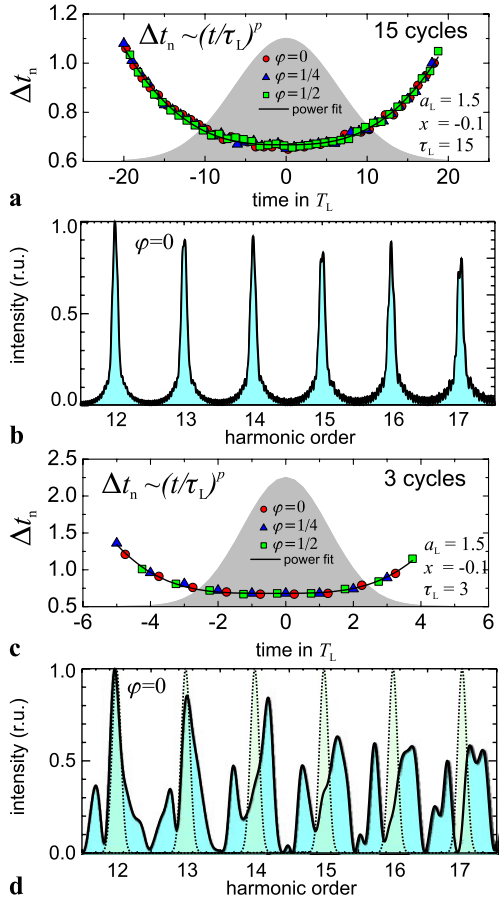

Fig. 9 Time delay between the nth positive-to-negative zero crossing of the E-field and the return of the individual electron bunches calculated for three different CE-phases for (**a**) a 15-cycle and (**c**) a 3-cycle pulse. The intensity of the driving pulses is given for reference. (**b**) and (**d**) show the harmonic spectra corresponding to pulse trains with as-pulses spaced according to the results shown in (**a**) and (**c**) respectively. For comparison, in (**d**) the spectrum for regularly spaced pulses is shown (*dashed line*)

very closely a $\Delta t_n(t,\varphi) = A|(t-(\varphi-\varphi_0))/\tau_L|^p + B$ dependency with A, B, φ_0 and p fitting parameters. The exponent p depends weakly on the pulse duration τ_L and for the two cases considered to a good approximation is constant and equal to 3. This is shown in Figs. 9(a) and 9(c) for the "long" and "short" pulse where Δt_n has been calculated for three CE-phases. It is seen that all values fall on the same curve indicating that it is the pulse envelope that determines Δt_n for each t. Note also that $\varphi_0 \neq 0$ because of the finite time spent by each electron in the vacuum.

4.2 Short-pulse spectra

To assess the influence of the unequal spacing on the spectra expected with laser intensities of $a_L = 1.5$ and for a given pulse duration τ_L we have calculated the spectrum $E_T(\omega)$ of a train of attosecond pulses unequally spaced in time given by:

$$E_T(\omega) = E_A(\omega)\sum_n E_L(t_n)e^{i\omega t_n}. \quad (2)$$

$E_A(\omega)$ represents the spectrum of a single electron burst of sub-cycle duration that excites plasma oscillations at all frequencies and it is assumed to be constant in the spectral range of interest. According to the CWE 3-step model, for a given φ the attosecond pulse within the nth cycle will occur at time $t_n = \Delta t_n(n,\varphi) + n - (\varphi - \varphi_0)$. Using (2) we have computed the spectrum for $\tau_L = 15$ (Fig. 9(b)) and $\tau_L = 3$ (Fig. 9(d)). For "long" pulses the spectrum exhibits regularly spaced individual harmonics in good agreement with the spectrum from previous experiments [1, 9, 13] and with properly "chirped" pulses (see Fig. 4). When the model is applied to a 3-cycle pulse (see Fig. 9(c)) the effect on the spectrum is striking (Fig. 9(d)). The individual harmonics are not only broadened but also are strongly distorted in shape. It is important to emphasize that despite the distortions the spectrum shown in Fig. 9(d) corresponds to a short train of individual attosecond pulses.

The key to the observed substructure in the harmonic spectrum lies in the intrinsic properties of the CWE generation process, which become perceptible because of the shortness of the driving laser pulse. To investigate the origin of the shot-to-shot variation in the spectrum and assess the impact of various parameters on the spectral structure of the emitted harmonics, we have conducted a parametric study for 3-cycle laser pulses using the model described previously. Using (2) we have calculated the expected spectra for the range $-0.5 \leq \varphi \leq 0.5$ and in the frequency range of the experimentally acquired spectra. Also, for the same laser pulse duration (3-cycles) we have performed PIC simulations using the code LPIC [3] and computed the emitted spectrum similarly for a range of the CEP. The thus obtained spectra for selected values of φ are depicted in Fig. 10 for both cases. We find that for specific values of φ the spectra calculated using the model and PIC simulation reproduce qualitatively remarkably well the features exhibited by the measured ones (see Fig. 3). As seen in Fig. 10 there is no exact correspondence of the spectrum for the same value of φ between model and simulation. This is attributed to the fact that while the PIC simulation computes everything self-consistently the model uses some simplifications. For example, the phase jump between the incident and the reflected wave at the plasma–vacuum interface depends on the local plasma density. This effect is taken into account self-consistently in the PIC simulation. In the model however, a constant phase jump of π is assumed.

According to the model, the time of emergence of the attosecond pulses crucially depends not only on CE-phase φ but also on the overall shape of the Δt_n curve. As expected,

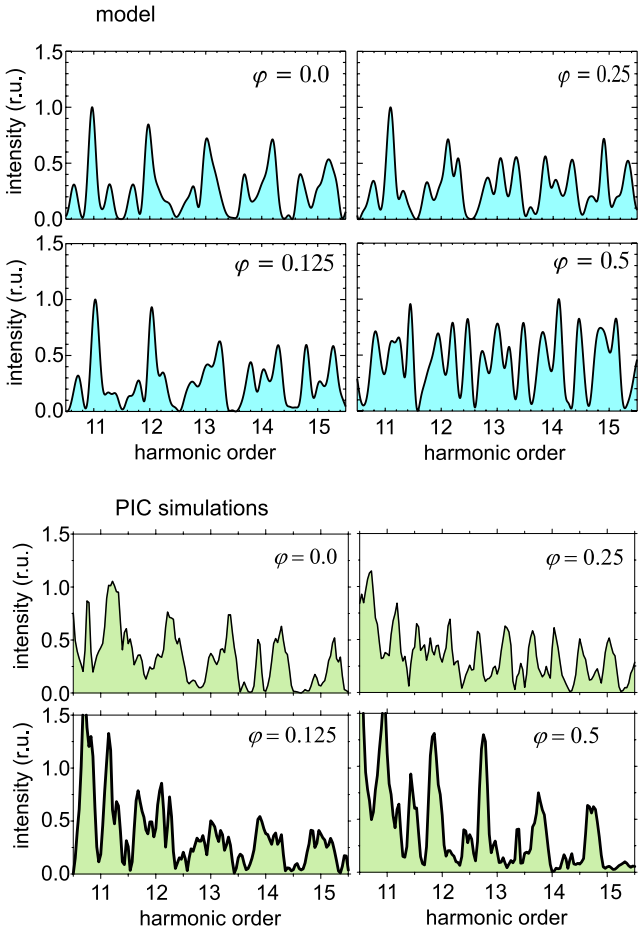

Fig. 10 *Top*: Modeled spectra obtained using (2) in the experimentally recorded range and for four different values of the normalized CE-phase φ. The spacing of the individual as-pulses was inferred from the data shown in Fig. 9. *Bottom*: PIC simulated spectra for the same values of the CE-phase

CEP variations have practically no influence on the harmonic spectrum of the 15-cycle pulse because most of the emitted attosecond pulses emanate in a time interval where the instantaneous intensity variation is negligible and as a result are equidistant. However, this is not the case for the 3-cycle pulses that were used in the experiments. An inspection of the analytical expression for the Δt_n curve shows immediately that its shape would also be affected by inherent pulse duration τ_L fluctuations, which, for our laser system, amount to 3%. Detailed model calculations indicate that this fluctuation level affects the relative amplitude of the peaks within each harmonic, whereas the overall shape (single-vs multi-peaked) is determined predominantly by the value of the CE-phase. A similar analysis shows that intensity (also in the 3% range) and scale-length fluctuations are affecting only the constants A and B and have negligible effect on the calculated spectrum. This suggests that shot-to-shot CEP fluctuations are chiefly responsible for the observed spectral structure.

4.3 Simulations on the effect of the polarization variation in the CWE regime

Previous reports [1, 9] have shown that, for purely p-polarized driver laser, the efficiency of harmonic generation varies with the intensity of the laser as $I_{XUV} \propto I_L^{0.4-1} \propto |E_L|^{0.8-2}$. Therefore, for mixed polarization (partially s-polarized and partially p-polarized) one expects that the harmonic intensity would similarly vary as $\propto E_{L,p}^{0.8-2}$ where $E_{L,p}$ is the p-component of the obliquely incident laser field. But from Fig. 6 it is evident, that in our case changing the plane of polarization from purely p to purely s, the efficiency is decreasing considerably faster than $|E_{L,p}|^2$. We have simulated the polarization variation using the PICWIG code and the results are shown in Fig. 6. The input parameters were the same as those given in Sect. 4.1 but the scale length in one case was kept constant at $L = 0.1\lambda_L$ (triangles in Fig. 6) while in the other was reduced progressively from $L = 0.1\lambda_L$ for $E_{L,s} = 0.3$ to $L = 0.04\lambda_L$ for $E_{L,s} = 1.0$ (circles in Fig. 6). As it is discussed later on, this is to simulate the effect of reduced absorption due to increasing s-polarized component in the incident field. As can be seen, the PIC simulations confirm the $|E_{L,p}|^2$ dependence for the case of fixed scale length. On the other hand the reduction of the scale length for increasing values of $E_{L,s}$ yields a dependence much closer to $|E_{L,p}|^4$ and to experimental results.

This result can be understood in terms of the different absorption mechanisms and their dependence on the polarization of the incident light. As has been reported in [36] the absorption of ultrashort laser pulses in overdense plasma is considerably lower in case of s-polarized light. The formation of preplasma and thus the resulting scale length depends on how much energy is absorbed in the time before the arrival of the peak of the pulse. It is reasonable to assume that the amount of absorption decreases as the part of s-polarized component in the incident pulse becomes more dominant. This in turn leads to smaller scale-length values. For reasons discussed by Dromey et al. [37], the consequence of that is the reduction of the harmonic emission due to the CWE mechanism.

In case of ellipticity variation the discrepancy to the simple scaling law shown in Fig. 7 can be attributed to more complex electron dynamics at the vacuum–plasma interface. The field component parallel to the target surface is influencing the trajectories of the extracted electrons. With increasing ellipticity of the incident electric field the electrons emanating from the target surface at different times will feel different parallel field components resulting in trajectories tilted under different angles to the target surface. Electrons reentering the plasma will therefore arrive under various angles which effectively reduces the bunching of these electrons and consequently diminishes plasma wave and with

this also harmonic production. Also in this case the absorption and therefore preplasma generation is different for p- and circularly polarized light, which is further affecting harmonic generation. The observation that for circular polarization there is still a 20% harmonics conversion is entirely different from the behavior of gas harmonics. The reason is that for circularly polarized laser light there still exists an electric field component in the plane of incidence, which remains the source of Brunel electrons for the CWE mechanism.

5 Conclusions

In summary, high-harmonic emission from solid targets was studied for the first time using a 3-cycle laser pulse in the multi-TW power scale. New aspects associated with the few-cycle emission have become apparent. We have identified the mechanism responsible for the substructures on the individual harmonics as due predominantly to the sub-cycle dynamics of the electrons responsible for harmonic generation.

The dependence of harmonic conversion on the polarization of the incoming laser beam—in the first approximation—corresponds to the expectations for the CWE mechanism. The high conversion to harmonics for a p-polarized beam drops very fast either by changing the direction of the linearly polarized radiation or by varying the ellipticity. This behavior might be advantageous for a possible approach to the generation of single attosecond pulses using the polarization gating technique. It appears that ellipticity variation is not an appropriate method because the conversion does not vanish even for purely circularly polarized radiation. On the other hand the fast decrease and high contrast when changing the polarization from p to s might open new possibilities for which an s–p–s polarization gating has to be developed.

Although the results obtained with our LWS laser system represent a decisive step forward, to reach the ultimate goal of isolated attosecond pulse generation with reproducible characteristics, further advances in laser technology like multi TW-scale laser systems delivering even shorter pulses with CEP stabilization and excellent characteristics are necessary. Provided that such high-performance laser systems become available, the effort should concentrate in reproducibly generating harmonics via the ROM mechanism, which appears to deliver a harmonic spectrum with superior characteristics, (e.g. higher photon energy, increased efficiency, smaller divergence, better phase locking properties) compared to that from the CWE mechanism.

Acknowledgements This work was funded in part by the DFG projects TR-18 and the MAP excellence cluster, by the LASERLAB-EUROPE, grant agreement # 228334, and by the associations EURATOM—MPI für Plasmaphysik and EURATOM—Hungarian Academy of Sciences. These co-authors gratefully acknowledges financial support as follows: J.M.M. by the Alexander-von-Humboldt Foundation and RFBR grants Nos. 08-02-01245-a and 08-02-01137-a, K.V. by the NKTH-OTKA (#74250) and Janos Bolyai Postdoctoral Fellowships, I.B.F. by the OTKA (#60531), and D.H. by Studienstiftung des deutschen Volkes.

References

1. Y. Nomura, R. Hörlein, P. Tzallas, B. Dromey, S. Rykovanov, Z. Major, J. Osterhoff, S. Karsch, L. Veisz, M. Zepf, D. Charalambidis, F. Krausz, G.D. Tsakiris, Nat. Phys. **5**, 124 (2009)
2. R. Hörlein, Y. Nomura, P. Tzallas, S. Rykovanov, B. Dromey, J. Osterhoff, Z. Major, S. Karsch, L. Veisz, M. Zepf, D. Charalambidis, F. Krausz, G.D. Tsakiris, New J. Phys. **12**, 043020 (2010)
3. R. Lichters, J. Meyer-ter Vehn, A. Pukhov, Phys. Plasmas **3**, 3425 (1996)
4. T. Baeva, S. Gordienko, A. Pukhov, Phys. Rev. E **74**, 046404 (2006)
5. Y.M. Mikhailova, V.T. Platonenko, S.G. Rykovanov, JETP Lett. **81**, 571 (2005)
6. G.D. Tsakiris, K. Eidmann, J. Meyer-ter Vehn, F. Krausz, New J. Phys. **8**, 19 (2006)
7. N.M. Naumova, C.P. Hauri, J.A. Nees, I.V. Sokolov, R. Lopez-Martens, G.A. Mourou, New J. Phys. **10**, 025022 (2008)
8. U. Teubner, P. Gibbon, Rev. Mod. Phys. **81**, 445 (2009)
9. F. Quéré, C. Thaury, P. Monot, S. Dobosz, P. Martin, J.-P. Geindre, P. Audebert, Phys. Rev. Lett. **96**, 125004 (2006)
10. B. Dromey, M. Zepf, A. Gopal, K. Lancaster, M.S. Wei, K. Krushelnick, M. Tatarakis, N. Vakakis, S. Moustaizis, R. Kodama, M. Tampo, C. Stoeckl, R. Clarke, H. Habara, D. Neely, S. Karsch, P. Norreys, Nat. Phys. **2**, 456 (2006)
11. B. Dromey, S. Kar, C. Bellei, D.C. Carroll, R.J. Clarke, J.S. Green, S. Kneip, K. Markey, S.R. Nagel, P.T. Simpson, L. Willingale, P. McKenna, D. Neely, Z. Najmudin, K. Krushelnick, P.A. Norreys, M. Zepf, Phys. Rev. Lett. **99**, 085001 (2007)
12. A. Tarasevitch, K. Lobov, C. Wuensche, D. von der Linde, Phys. Rev. Lett. **98**, 103902 (2007)
13. F. Quéré, C. Thaury, J.-P. Geindre, G. Bonnaud, P. Monot, P. Martin, Phys. Rev. Lett. **100**, 095004 (2008)
14. C. Thaury, H. George, F. Quéré, R. Loch, J.-P. Geindre, P. Monot, P. Martin, Nat. Phys. **4**, 631 (2008)
15. B. Dromey, D. Adams, R. Hörlein, Y. Nomura, S.G. Rykovanov, D.C. Caroll, P.S. Foster, S. Kar, K. Markey, P. McKenna, D. Neely, M. Geissler, G.D. Tsakiris, M. Zepf, Nat. Phys. **5**, 146 (2009)
16. M. Hentschel, R. Kienberger, C. Spielmann, G.A. Reider, N. Milosevic, T. Brabec, P. Corkum, U. Heinzmann, M. Drescher, F. Krausz, Nature **414**, 509 (2001)
17. F. Krausz, M. Ivanov, Rev. Mod. Phys. **81**, 163 (2009)
18. P. Tzallas, E. Skantzakis, E.P. Benis, G.D. Tsakiris, D. Charalambidis, Nat. Phys. **3**, 846 (2007)
19. T. Baeva, S. Gordienko, A. Pukhov, Phys. Rev. E **74**, 065401 (2006)
20. S. Rykovanov, M. Geissler, J. Meyer-ter Vehn, G.D. Tsakiris, New J. Phys. **10**, 025025 (2008)
21. A. Baltuska, M. Uiberacker, E. Goulielmakis, R. Kienberger, V.S. Yakovlev, T. Udem, T.W. Hänsch, F. Krausz, IEEE J. Sel. Top. Quantum Electron. **9**, 972 (2003)
22. F. Tavella, Y. Nomura, L. Veisz, V. Pervak, A. Marcinkevicius, F. Krausz, Opt. Lett. **32**, 2227 (2007)
23. D. Herrmann, L. Veisz, R. Tautz, F. Tavella, K. Schmid, V. Pervak, F. Krausz, Opt. Lett. **34**, 2459 (2009)

24. C. Thaury, F. Quéré, J.-P. Geindre, A. Levy, T. Ceccotti, P. Monot, M. Bougeard, F. Réau, P. d'Oliveira, P. Audebert, R. Marjoribanks, P. Martin, Nat. Phys. **3**, 424 (2007)
25. P. Gibbon, Phys. Rev. Lett. **76**, 50 (1996)
26. K. Gál, S. Varró, Opt. Commun. **198**, 419 (2001)
27. L.A. Gizzi, D. Giulietti, A. Giulietti, P. Audebert, S. Bastiani, J.P. Geindre, A. Mysyrowicz, Phys. Rev. Lett. **76**, 2278 (1996)
28. E. Rácz, I.B. Földes, G. Kocsis, G. Veres, K. Eidmann, S. Szatmári, Appl. Phys. B, Lasers Opt. **82**, 13 (2006)
29. P.A. Norreys, M. Zepf, S. Moustaizis, A.P. Fews, J. Zhang, P. Lee, M. Bakarezos, C.N. Danson, A. Dyson, P. Gibbon, P. Loukakos, D. Neely, F.N. Walsh, J.S. Wark, A.E. Dangor, Phys. Rev. Lett. **76**, 1832 (1996)
30. G. Veres, J.S. Bakos, I.B. Földes, K. Gál, Z. Juhász, G. Kocsis, S. Szatmári, Europhys. Lett. **48**, 390 (1999)
31. R.A. Ganeev, A. Ishizawa, T. Kanai, T. Ozaki, H. Kuroda, Opt. Commun. **227**, 175 (2003)
32. P.B. Corkum, Phys. Rev. Lett. **71**, 1994 (1993)
33. F. Brunel, Phys. Rev. Lett. **59**, 52 (1987)
34. Z.-M. Sheng, K. Mima, J. Zhang, H. Sanuki, Phys. Rev. Lett. **94**, 095003 (2005)
35. F. Brandl, B. Hidding, J. Osterholz, D. Hemmers, A. Karmakar, A. Pukhov, G. Pretzler, Phys. Rev. Lett. **102**, 195001 (2009)
36. M. Cerchez, R. Jung, J. Osterholz, T. Toncian, O. Willi, Phys. Rev. Lett. **100**, 245001 (2008)
37. B. Dromey, S.G. Rykovanov, D. Adams, R. Hörlein, Y. Nomura, D.C. Caroll, P.S. Foster, S. Kar, K. Markey, P. McKenna, D. Neely, M. Geissler, G.D. Tsakiris, M. Zepf, Phys. Rev. Lett. **102**, 225002 (2009)